POLİTEKNİK DERGİSİ

JOURNAL of POLYTECHNIC

ISSN: 1302-0900 (PRINT), ISSN: 2147-9429 (ONLINE)
URL: http://dergipark.org.tr/politeknik

Analysis of directional stability of a quadcopter for different propeller designs using experimental and computational fluid dynamics applications

Bir quadcopter'ın yön kararlılığının farklı pervane tasarımları kullanarak deneysel ve hesaplamalı akışkanlar dinamiği ile analizi

***Yazar(lar) (Author(s))**: Yahya ÇELEBİ[1], Hüseyin AYDIN[2]*

ORCID[1]: 0000-0002-4686-9794

ORCID[2]: 0000-0002-5415-0405

To cite to this article: Çelebi Y. ve Aydın H., "Analysis of Directional Stability of A Quadcopter for Different Propeller Designs Using Experimental And Computational Fluid Dynamics Applications", ***Journal of Polytechnic***, 29(1):290110:1-12 (2026).

Bu makaleye şu şekilde atıfta bulunabilirsiniz: Çelebi Y. ve Aydın H., "Analysis of Directional Stability of A Quadcopter for Different Propeller Designs Using Experimental And Computational Fluid Dynamics Applications", ***Politeknik Dergisi***, 29(1):290110:1-12 (2026).

Erişim linki (To link to this article): http://dergipark.org.tr/politeknik/archive

DOI: 10.2339/politeknik.1553077

Analysis of Directional Stability of A Quadcopter for Different Propeller Designs Using Experimental and Computational Fluid Dynamics Applications

Highlights

- *Four new propeller designs were designed and tested for a quadcopter.*
- *CFD analysis was done to verify designs before 3D printing and real-world testing.*
- *All new propellers showed excellent directional stability in flight tests.*
- *NACA4412 and NLF0115 propellers demonstrated the best overall performance.*
- *This study emphasizes the potential of custom propeller designs for improving quadcopter performance.*

Graphical Abstract

This study designed and tested four new propeller types for quadcopters, aiming to improve stability. Both computational and experiments showed good performance across all designs, with NACA4412 and NLF0115 propellers showing superior results. The research demonstrates the significant potential of custom propellers in enhancing quadcopter performance.

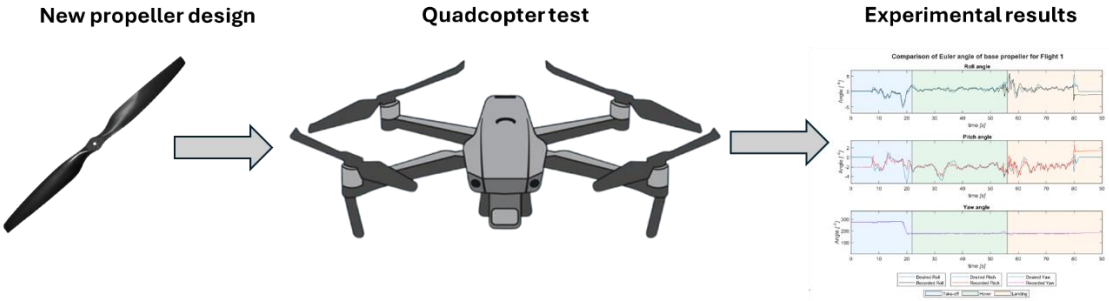

Figure. Graphical abstract of the study

Aim

Design and test new propeller types for quadcopter drones to improve directional stability.

Design & Methodology

Four propellers were designed and then analyzed using CFD, manufactured with 3D printing, and evaluated through comprehensive flight testing.

Originality

Focus on designing new propellers specifically for quadcopters, rather than analyzing commercial ones.

Findings

All designs showed good stability. NACA4412 and NLF0115 propellers performed the best, with improved power consumption.

Conclusion

Custom propeller designs can optimize quadcopter performance. Both CFD and experimental analysis are crucial in the design process.

Declaration of Ethical Standards

The author(s) of this article declare that the materials and methods used in this study do not require ethical committee permission and/or legal-special permission.

Analysis of Directional Stability of A Quadcopter for Different Propeller Designs Using Experimental and Computational Fluid Dynamics Applications

Araştırma Makalesi / Research Article

Yahya ÇELEBİ[1*], Hüseyin AYDIN[2]

[1]Şırnak University, Department of Motor Vehicles and Transportation Technologies, Şırnak, Türkiye, 73000
[2]Türkiye Batman University, Department of Mechanical Engineering, Batman, Türkiye, 72060

(Geliş/Received : 19.09.2024 ; Kabul/Accepted : 12.05.2025 ; Erken Görünüm/Early View : 22.05.2025)

ABSTRACT

In recent years, unmanned aerial vehicles (UAVs), popularly referred to as drones, have been widely adopted across various industries. Among these, quadcopter is the most popular type of UAV characterized by its four propellers. This study focuses on enhancing quadcopter directional stability through the design and testing of four novel propeller types based on DAE51, MH42, NACA4412, and NLF0115 airfoils. ANSYS Fluent simulations were performed to evaluate the accuracy of propeller performance predictions. Methodology verification conducted using an APC 10x7 propeller demonstrated error rates below 5.2% for thrust coefficients. Experimental analyses were performed in outdoor environment to account for realistic wind effects on propeller performance. The custom-designed propellers were compared to baseline quadcopter propeller. Results indicated no significant discrepancies between desired and observed values for pitch, roll, yaw angles, altitude, or vibration levels. Power consumption tests revealed that NACA4412 and NLF0115 propellers used 7% and 3.6% less power than original propellers, while DAE51 and MH42 propellers consumed 6.7% and 20% more power, respectively. NACA4412 and NLF0115 designs demonstrated particularly favorable performance characteristics, offering improved power efficiency while maintaining excellent directional stability.

Keywords: Directional stability, drone, uav, propeller, quadcopter.

Bir Quadcopter'ın Yön Kararlılığının Farklı Pervane Tasarımları Kullanarak Deneysel ve Hesaplamalı Akışkanlar Dinamiği İle Analizi

ÖZ

Günümüzde, yaygın olarak drone olarak bilinen insansız hava araçları (İHA) çeşitli sektörlerde geniş çapta benimsenmiştir. Bunlar arasında, dört pervanesi olan dörtuçar, en popüler İHA türüdür. Bu çalışma, DAE51, MH42, NACA4412 ve NLF0115 kanat profillerinden dört yeni pervane tipinin tasarımı ve test edilmesi ile dörtuçarın yön kararlılığını geliştirmeye odaklanmaktadır. Pervane performans tahminlerinin doğruluğunu değerlendirmek için ANSYS Fluent simülasyonları gerçekleştirilmiştir. Metodoloji doğrulaması için APC 10x7 pervane kullanılmış ve itme katsayısı sapma oranı %5,2'nin altında elde edilmiştir. Pervanelerin performansı üzerinde oluşan rüzgar etkilerini hesaba katmak için deneysel analizler açık havada gerçekleştirilmiştir. Tasarım pervaneler, orijinal dörtuçar pervanesi ile karşılaştırılmıştır. Testler sonucunda elde edilen veriler, yunuslama, yuvarlanma, sapma açıları, irtifa veya titreşim seviyeleri için istenen ve gözlenen değerler arasında önemli bir fark olmadığını göstermiştir. Güç tüketimi testleri, NACA4412 ve NLF0115 pervanelerinin orijinal pervaneden %7 ve %3,6 daha az güç kullandığını, DAE51 ve MH42 pervanelerinin ise sırasıyla %6,7 ve %20 daha fazla güç tükettiğini ortaya koymuştur. NACA4412 ve NLF0115 tasarımları, daha iyi yön kararlılığını gösterirken, aynı zamanda yüksek verimlilik sunarak üstün performans göstermiştir.

Anahtar Kelimeler: Doğrultu kararlılığı, drone, iha, pervane, dörtuçar.

1. INTRODUCTION

Throughout history, societies valued humans primarily as labor sources until the industrial revolution transformed this paradigm. Technological advancement has enhanced system efficiency while reducing manual labor requirements, removing humans from hazardous environments and enabling algorithm-based control systems. Modern unmanned vehicles work without direct human control and fall into different groups such as unmanned ground vehicles, unmanned aerial vehicles (UAV), unmanned space vehicles, unmanned underwater vehicles, and unmanned surface vehicles [1].

Technological progress and reduced electronic equipment costs have contributed to the growth of the UAV sector [2], and the market now offers numerous open-source and commercial UAV options. Commercial equipment typically restricts software and hardware modifications, but open-source alternatives provide researchers and developers greater freedom. Open-source equipment remains affordable and flexible, so it

*Sorumlu Yazar (Corresponding Author)
e-posta : yahya.celebi@outlook.com

has become popular among researchers and hobbyists [3]. Today, UAVs are used in various areas including intelligence gathering, border control, enemy detection, ammunition transport in military services, fault detection and gas measurement in power generation, as well as in agriculture, mapping, geological field detection, and disaster management. Furthermore, ongoing research and development efforts are exploring the usage of UAVs on numerous areas such as first aid (search and rescue) and traffic control [4–6].

UAVs are classified into three categories that are fixed-wing, rotary-wing, and hybrid [7]. Fixed-wing UAVs utilize aerodynamic lift generated by their wings during forward motion. These UAVs are powered by either internal combustion engines or electric motors, offering excellent fuel efficiency due to their single motor design. While fixed-wing UAVs excel in flight range and endurance, they cannot perform vertical takeoff and landing, requiring substantial space for ground operations, which represents their primary limitation. Rotary-wing UAVs generate lift through continuously rotating propellers. This design enables a stationary frame that allows precise hovering capabilities, and vertical takeoff and landing in restricted spaces. However, rotary-wing UAVs have higher production costs than fixed-wing UAVs due to their complex design requiring multiple motors, electronic controllers, and propellers. Hybrid UAVs aim to combine the advantages of both fixed-wing and rotary-wing of UAVs. But their development is progressing slowly [8,9].

Rodrigues et al. [10] studied package delivery effects on quadcopter power consumption, altitude, payload and ground speed using a DJI Matrice 100 during 11 hours of flight tests, analyzing results through Euler angles and altitude measurements. Su et al. [11] improved UAV stability by combining barometer and accelerometer sensors, achieving 3.67% displacement between sensors and demonstrating more accurate movement when both sensors operated together. Azizan and Sapit [12] designed multiple propellers with varying angles (constant vs. twisted) and used Ansys Fluent CFD analysis to determine the third design with twisted blades generated highest thrust at 6000 rpm. Sanchez [13] designed six propellers using different airfoils (AH 79-100 A, GM15, FX 63-120, GOE 358, SA7026), 3D-printed them, used XFOIL to determine lift-to-drag ratios, and found SA7026 airfoil propellers produced lowest noise. Dim et al. [14] built a drone with F450 frame using Ardupilot and Pixhawk control boards, programmed autonomous routes, and determined Pixhawk 4 controllers provided superior flight stability performance. Ghaffari [15] conducted numerical studies on a 25kg-payload octocopter using 3D scanning to assess propeller dimensions, with CFD analysis revealing 0.65 axial separation maximized propeller efficiency and flight time. Alabaş and Nacaklı [16] performed CFD analysis on commercial APC 10x6 four-blade propellers using Multiple Reference modeling with 6x8D stationary domain and 1.06x0.8D rotating region, achieving results within 2.97% of experimental data.

While extensive research exists on UAVs and commercial propellers, there remains a significant gap in the literature regarding custom propeller designs specifically optimized for quadcopters. Most studies focus on analyzing existing commercial propellers rather than developing new designs. This study addresses this gap by designing and testing four novel propeller types based on DAE51, MH42, NACA4412, and NLF0115 airfoils, which were selected for their reported efficiency at low Reynolds numbers (Re < 100,000). The research employs a comprehensive methodology combining theoretical calculations, computational fluid dynamics (CFD) analysis, and real-world flight testing to evaluate directional stability, power consumption, and overall performance. This integrated approach not only validates the effectiveness of custom propeller designs for quadcopters but also establishes a systematic framework for propeller development that can significantly enhance UAV performance while reducing development costs and time. By focusing on both computational validation and experimental verification, this study provides valuable insights for researchers and manufacturers seeking to optimize quadcopter propulsion systems.

2. MATERIAL and METHOD

To define propeller performance, three key parameters are utilized which are thrust coefficient (C_T), torque coefficient (C_Q), and efficiency (η) are defined in Eqs. (1-3) [17]. In these equations, Q (N/m) is torque, n (rps) is the rotational speed of the propeller and D (m) is the diameter of the propeller. These parameters provide standardized metrics for evaluating and comparing different propeller designs under various operating conditions. The relative percentage error of the C_T and C_Q can be calculated by the Equations (4-5) [18].

$$C_Q = \frac{Q}{\rho n^2 D^5} \tag{1}$$

$$C_T = \frac{T}{\rho n^2 D^4} \tag{2}$$

$$\eta = \frac{C_T}{C_P} J \tag{3}$$

$$\Delta C_Q(\%) = \frac{C_{Q,CFD} - C_{Q,Exp.}}{C_{Q,Exp.}} x100 \tag{4}$$

$$\Delta C_T(\%) = \frac{C_{T,CFD} - C_{T,Exp.}}{C_{T,Exp.}} x100 \tag{5}$$

2.1. Quadcopter and Propeller Calculations

The designer can choose the battery, motors, and propellers when designing a quadcopter for collecting purposes. However, the choice of motor and propeller should be made in consideration of the other components. The total mass of the quadcopter components including frame, propeller, motor, esc, battery, GPS, flight controller, anemometer and interconnects was weighed as 1.432 kg.

The number of battery cell determines the maximum thrust force for the UAV. All propellers produce an equal amount of thrust during takeoff and landing. Because the angles of roll, pitch and yaw are zero [19]. The specifications of the components used for thrust calculations of the UAV are provided in Table 1.

Table 1. Values of the components used for the thrust calculation.

Specification	Value
Nominal battery voltage	11.1 V
K_V value of motor	380 K_V
Reference propeller (diameter x pitch)	10x45 in

In order to calculate the values for quadcopter, the peak thrust force must be determined for each motor at full power. Researchers often consider this ratio to be 1.5 or 1.75 [20]. For this study, a thrust-to-weight ratio of 1.5 is selected for thrust calculation which is deemed sufficient for this UAV. The thrust force is calculated using the equation below [20].

$$T = \frac{I_K \cdot m \cdot g}{i} \tag{6}$$

Where T is the thrust force, I_K is the thrust-to-weight ratio, m is the mass of the UAV, g is gravity and i is the number of rotors. Minimum thrust force required for the UAV is determined by Equation (7).

$$T = \frac{1.5\ x\ 1.432\ \text{kg}\ x\ 9.81\ \text{kg/ms}^2}{4} = 5.2679\ \text{N} \tag{7}$$

As propeller design has not been carried out at this stage, the surface area of a reference propeller (DJI 1045) proposed for the engine and frame combination was used for calculations. The surface area of the DJI 10x45 is measured as 0.010664 m^2. When the air density (where ρ=1.225 kg/m^3) along with thrust force and the surface area of the reference propeller are put into the equation, theoretical velocity of the UAV can be derived as follows.

$$V = \sqrt{\frac{T}{2\rho A}} = \sqrt{\frac{5.2679}{2 \times 1.225 \times \pi \times 0.010664}} = 8.0112\ m/s \tag{8}$$

The airfoils selected for this research included DAE51, NLF0115, NACA4412 and MH42. Researchers have noted that these airfoils exhibit high efficiency at low Reynolds numbers (Re < 100,000) [21–24]. The appearance of these airfoils is depicted in Figure 1.

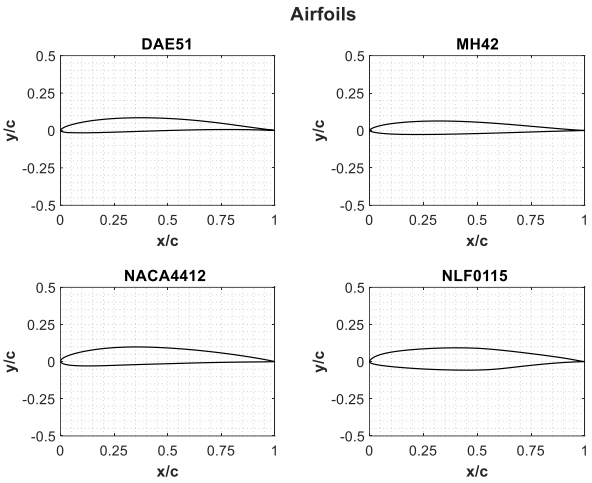

Figure 1. Appearance of airfoils.

In the design process, high lift coefficient (C_L), low drag coefficient (C_D), and the optimal aerodynamic efficiency (C_L/C_D) dependent on these two parameters [25]. The JBLADE software was employed to calculate the C_L/C_D ratios corresponding to the angle of attack. The X and Y coordinates of the airfoils were inputted into the software prior to its usage. Once the profile coordinates and ambient conditions have been uploaded into the software, a graph representing C_D, α and C_L/C_D ratios was generated for Re=10^5. C_L and C_D values were obtained in the range of –10° and +20° of angle of attack. In Figure 2, C_L/C_D ratios corresponding to the angle of attack are provided for each profile at Re=10^5.

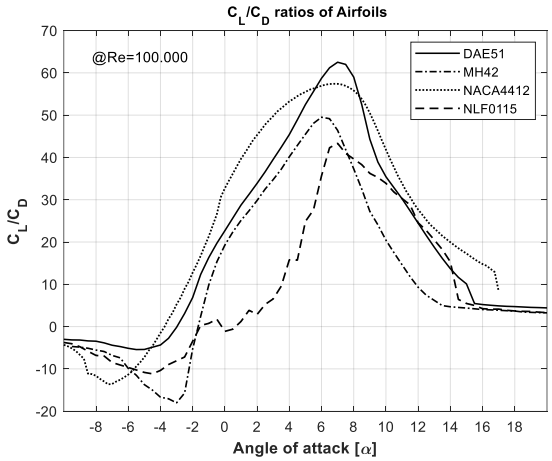

Figure 2. C_L/C_D ratios versus the angle of attack of the airfoils.

This software utilizes mathematical calculations to determine the angle of attack based on C_L/C_D ratios. The propeller performance data for the DAE51, NLF0115, NACA4412 and MH42 profiles are presented in

Table 2.

Table 2. Comparison of performance calculation of the airfoils.

DAE51				NLF0115				NACA4412				MH42			
α	C_L	C_D	C_L/C_D	α	C_L	C_D	C_L/C_D	α	C_L	C_D	C_L/C_D	α	C_L	C_D	C_L/C_D
7.00	1.20	0.020	62.52	7.00	0.88	0.020	43.33	6.75	1.14	0.019	57.41	6.00	0.82	0.020	49.51

The preliminary design conditions for the propeller included a propeller diameter, an air density, a blade number, and rotational speeds. Specifically, the NACA4412 and NLF0115 profiles were designed for operation at 6000 rpm, while the DAE51 and MH42 profiles were designed for operation at 5500 rpm rotational speed. It is important to note that when determining the thrust force, the rotational speed and chord length have an inverse relationship.

The values of the chord and twist distribution along the blade length were obtained using QMIL software, developed by Mark Drela from Massachusetts University. QMIL software is primarily used for propeller design based on predetermined preliminary design parameters [26]. The software provided values for the element length, radial length of the element, angle of twist, and chord length for each airfoil. The calculated design parameters obtained from QMIL for all the airfoils are presented in

Table **3**. Using these design calculations, the solid models of the propellers can be generated.

Table 3. Calculations of the design parameters for the airfoils.

Element number		1	2	3	4	5	6	7	8	9	10	11
r (mm)		18.7	30.1	41.5	52.9	64.3	75.7	87.1	98.5	109.9	121.3	127
DAE51	c (mm)	66.2	43.2	31.9	25.2	20.8	17.6	15.2	13	10.5	6.5	3.9
	β (°)	36.5	25.9	20.5	17.3	15.2	13.7	12.6	11.7	11	10.4	10.2
MH42	c (mm)	56.2	51.6	43.4	36.4	30.7	26.1	22.1	18.3	14.1	8.2	4.6
	β (°)	50.5	37.2	29.3	24.2	20.7	18.2	16.3	14.9	13.7	12.7	12.3
NACA4412	c (mm)	43.5	41.9	36.2	30.7	26	22.1	18.7	15.3	11.7	6.7	3.7
	β (°)	59.8	46.3	37.9	32.5	28.6	25.9	23.7	22.1	20.7	19.6	19.2
NLF0115	c (mm)	53.2	48.8	41	34.4	29.1	24.7	20.9	17.3	13.3	7.7	4.3
	β (°)	55	41.6	33.7	28.7	25.2	22.7	20.8	19.3	18.1	17.1	16.7

Ultimaker CURA is a software program used for slicing solid models designed for 3D printing [27]. Initially, the propellers were sliced using this software and then 3D printed with the assistance of a memory card. A visual representation of the printed propellers is presented in Figure 3, with 3a displaying the final assembled propeller and 3b showing the raw printed propeller.

Figure 3. View of the printed propellers.

2.2. Experimental Setup

The quadcopter used in the tests was assembled with the following components: Pixhawk 4 flight controller, GPS, F450 frame, DJI 10x45 propellers, Emax XA2212 brushless motors, HobbyWing XRotor 40A electronic speed controllers, TE MS4525DO digital anemometer, Turnigy Graphane 3S Lipo battery, Frsky Taranis Q X7 remote controller, Frsky R9M radio transmitter module, and Pixhawk 4 power module. Prior to the flight tests, several preparations were made, including balancing the propellers and battery, and calibrating the ESC, accelerometer, and compass. Experimental setup diagram used in the study is presented in Figure 4.

Pixhawk determines the position, acceleration, and orientation of the quadcopter using an extended Kalman filter, which processes data from various sensors including the gyroscope, barometer, accelerometer, GPS,

anemometer, and compass, as described on their website. The control board records flight data such as roll, pitch, and yaw angles, collects altitude information, and monitors vibration levels. Power consumption is measured using a digital power meter, while wind speed is recorded by an external anemometer that mounted on the quadcopter.

Autonomous flight plans were created and uploaded to the vehicle using Mission Planner software. Then, outdoor flight experiments were conducted for each propeller. The results of the outdoor flight tests were recorded on the SD card via the flight controller. The flight started with takeoff to 10m, continued with ascent to 20m for hovering, and ended with direct landing.

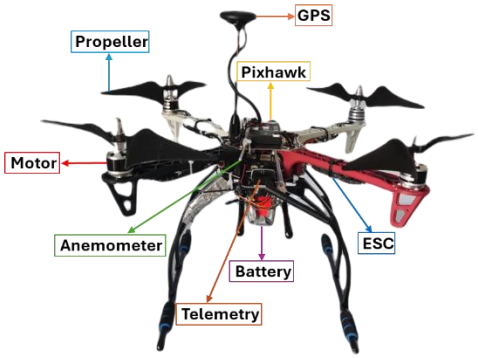

Figure 4. Experimental setup diagram.

3. COMPUTATIONAL SETUP

3.1. CFD Independence

Before conducting CFD calculations on a propeller model, it is essential to verify and validate the method. This involves assessing the suitability of the mesh, the rotating fluid region, and the chosen turbulent model. Validation is typically performed by comparing the CFD results with existing sets of experimental or CFD results. The ANSYS Fluent software was utilized for the CFD calculations. To validate the CFD model, experimental performance results from the literature were used to create a model, and then comparisons were made. Subsequently, the test propellers were analyzed under the same conditions using CFD.

For the verification and validation process, a small-scale propeller called APC 10x7 Slow Flyer was employed. This propeller has a 10-inch diameter and 7-inch pitch and is documented in the literature with experimental results under various test conditions. The verification and validation of the propeller were carried out at a rotational speed of 3008 rpm. The CFD results for the torque coefficient, pressure coefficient, and efficiency of the APC 10x7 Slow Flyer were compared with the experimental data, and the error rate was determined. A visual representation of the APC 10x7 Slow Flyer is presented in Figure 5.

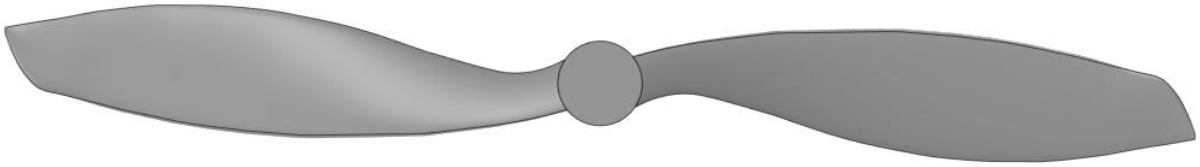

Figure 5. View of APC 10x7 Slow Flyer.

The Multiple Reference Frame (MRF) model approach was applied to predict the flow around the propeller. The flow model was developed using ANSYS Design Modeller, where two distinct domains were established, with the propeller positioned at the center. The outer cylinder serves as the stationary reference frame, with dimensions equivalent to a diameter and length of 17 times the propeller's diameter (17 D). The inner cylinder functions as the moving reference frame, with a diameter equal to 1.5 times the propeller's diameter and a length of 1.15 times the propeller's diameter (1.5 D x 1.15 D). The flow schematic illustrating both the inner and outer domains is depicted in Figure 6.

The mesh generation process was carried out using ANSYS Fluent Meshing, and a poly-hexcore meshing type was employed. The choice of poly-hexcore meshing offers the advantage of requiring fewer elements, thereby facilitating faster solution convergence [28]. The mesh size gradually increased from the propeller surface outward into the outer domain. The mesh distribution on the propeller surface is illustrated in Figure 7.

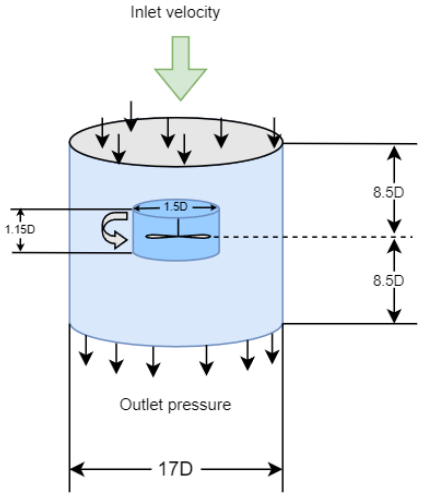

Figure 6. Fluid domain.

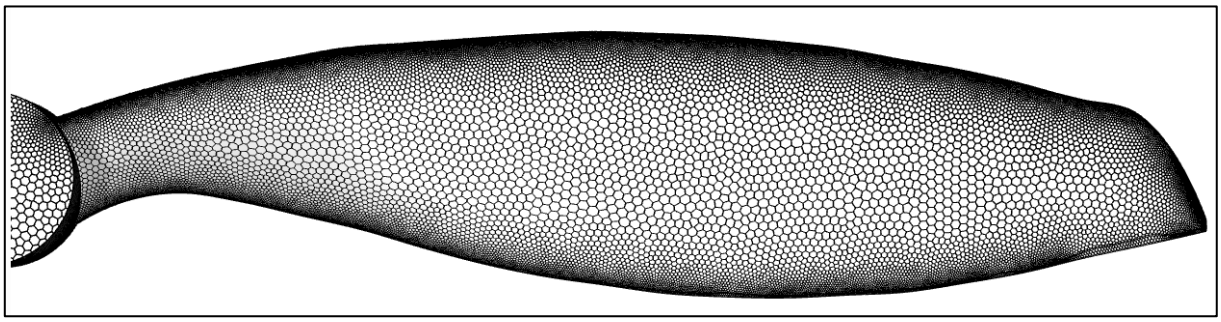

Figure 7. View of the mesh distribution on the propeller surface.

The first layer thickness is calculated with the equation below. In the equation, y is the first layer thickness (mm), $y+$ is the number of layers and μ is the dynamic viscosity (Pa.s) [16];

$$y = \frac{y^{+}\mu}{\rho u_{*}}$$

Table 4. Boundary conditions for validation.

Property	Value
Turbulence model	SST k-ω
Fluid	Air
The density of fluid (kg/m3)	1.225
Inlet velocity (m/s)	8.0112
Outlet pressure (Pa)	0
Propeller domain	'None Slip Wall' condition

Using the aforementioned equation with a growth rate of 1.2 and a total of 5 layers, the first layer thickness is calculated to be 0.1798 mm. The domain of the propeller and the hub was described as no slip wall condition. The selection of an appropriate turbulence model is crucial for ensuring both experimental validation and solution accuracy [29]. SST k-ω turbulence model was used for this study because it shows very close results to the experimental data. The parameters of the boundary conditions are given in Table 4.

3.2. Independence Analysis

Independence analysis is a crucial step in numerical analysis. It verifies that the simulation results remain consistent even as the number of elements increases. This process is essential for optimizing computational resources and avoiding excessive element usage. To conduct independence analysis, the initial model was created with a relatively low number of elements. The number of elements was then systematically increased until the results exhibited no significant changes. Mesh independence analysis was performed at a specific rotational speed of 3008 rpm and an advance coefficient of 0.628. The quality of the mesh and numerical data for the mesh of APC 10x7 Slow Flyer, relevant to the mesh independence study, is provided in Table 5

.

Table 5. Mesh quality and numerical data for validation at J=0.628.

Mesh	Cells	Faces	Nodes	Skewness	Orthogonal quality	Error (%)		
						C_T	C_Q	η
Fine	4,786,422	20,656,050	11,552,972	0.76	0.17	0.034	5.157	–4.878
Coarse	3,141,866	13,621,624	7,671,163	0.72	0.21	0.168	5.348	–4.923
Standard	1,955,128	8,496,191	4,811,612	0.68	0.34	0.727	6.035	–5.011

The analysis was conducted at an advance coefficient of 0.628 to assess mesh independence. Based on the data obtained from the mesh independence analysis, there is a slight change of thrust and torque forces with the number of elements when the mesh is increased.

In order to ensure a comprehensive comparison using the standard meshing parameters, the performance results obtained from CFD simulations for the APC 10x7 Slow Flyer were validated against experimental results at advance coefficients of 0.282, 0.423, and 0.799 as well. Figure 8 presents a comparison between numerical and experimental results of C_T, C_Q and η as functions of advance coefficients. The figure illustrates a close alignment between the CFD and experimental results, with only minor differences observed. These findings

suggest that the standard meshing approach employed is adequate for accurately predicting C_T, C_Q and η.

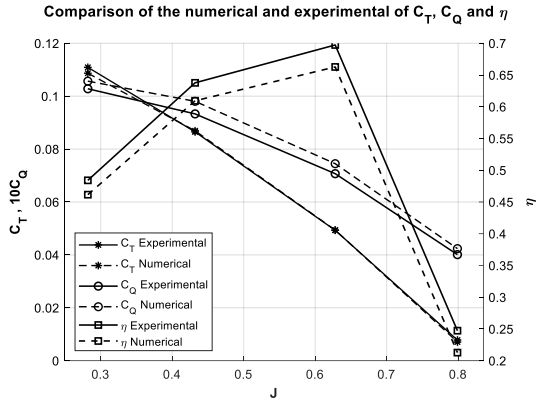

Figure 8. Comparison of the CFD and experimental data of APC 10x7.

4. RESULTS and DISCUSSION

4.1. CFD Analysis

Mesh generation plays a crucial role in influencing CFD performance, the rate of convergence, and computational analysis time. In this study, cell sizes within the mesh were initially set to default values and then systematically reduced until the results achieved the desired level of accuracy. A refined mesh was specifically applied to the surface of the propeller. For the validation model, the mesh settings were customized, necessitating manual adjustments to enhance mesh quality.

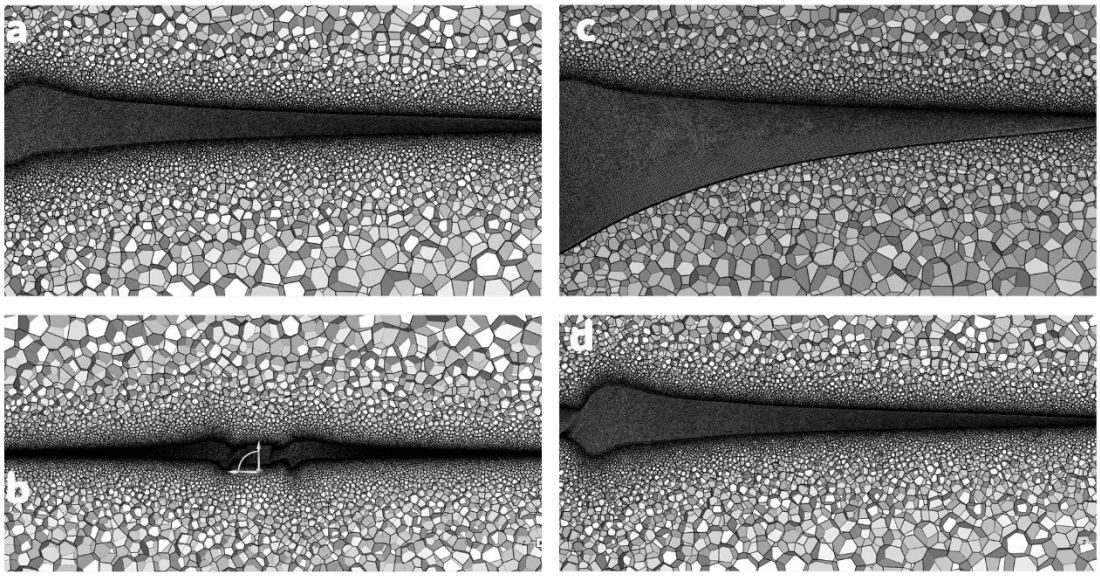

Figure 9. Mesh generation on the propeller surfaces.

Table 6. The mesh properties for the designed propellers.

Property /Propeller	Cells	Faces	Nodes	Skewness	Orthogonal quality
DAE51	2,607,804	14,315,397	10,159,102	0.69	0.30
MH42	2,997,781	16,222,689	11,987,005	0.75	0.24
NACA4412	2,578,445	14,040,433	9,894,974	0.75	0.24
NLF0115	2,894,968	15,688,078	11,021,857	0.79	0.20

Figure 9 illustrates the mesh generation on the propeller surfaces. The surface meshes are shown for DAE51 (**Figure 9**a), MH42 (**Figure 9**b), NACA4412 (**Figure 9**c), and NLF0115 (**Figure 9**d) propeller designs. For a high-quality mesh structure, the skewness value should be close to 0, while the orthogonal quality should be close to 1 [30]. The mesh properties for the designed propellers are given **Table 6**.

The calculation of the thrust force for the quadcopter was derived using a theoretical method. During this theoretical calculation, the minimum thrust force required for the quadcopter to overcome aerodynamic loads was determined. It is important to note that thrust force has a significant impact on the stability and flight characteristics of the UAV.

Table 7 presents the disparities between the theoretical and CFD methods for calculating thrust coefficient in the designed propellers. The differences between the theoretical and CFD calculations of the required thrust for the DAE51, MH42, NACA4412, and NLF0115 propellers are –3.935%, –5.11%, –5.80%, and –6.73%, respectively. These results indicate that the thrust force

generated by the designed propellers for the UAV will be very close to the calculated values, with only minor differences.

Table 7. The comparison of the theoretical and CFD data for the designed propeller.

Property/Propeller	DAE51	MH42	NACA4412	NLF0115
Theoretical	0.1487	0.1487	0.1033	0.1033
CFD	0.1428	0.1411	0.0973	0.0963
Error % C_T	–3.935%	–5.11%	–5.80%	–6.73%

4.2. Flight Results

4.2.1. Base propeller

Figure 10 depicts the variation of the desired and recorded Euler angle for the base propeller. The graphs in the figure illustrated that there is only a slight difference between the desired and recorded angles of pitch, roll, and yaw. In simpler terms, it indicates that the UAV closely followed the intended flight path during the flight. During the landing phase, a noticeable displacement occurred in both the pitch and roll angles. The most significant deviation observed was 8.15° for the roll angle and 2.14° for the pitch angle. In contrast, the yaw angle remained relatively stable and closely followed the intended route, with the highest deviation in yaw angle recorded at 14.07°

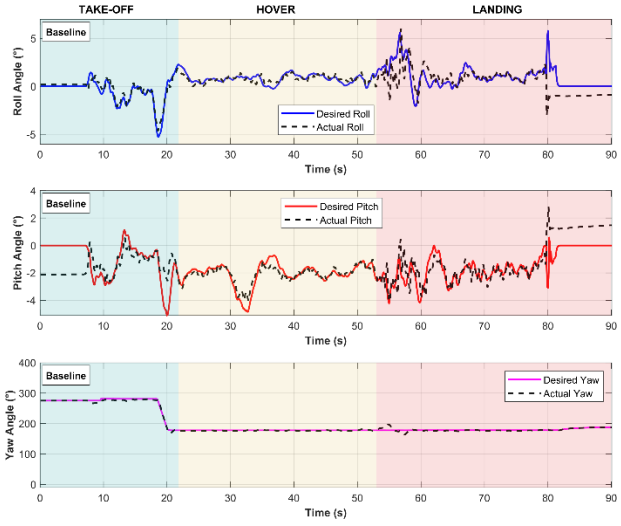

Figure 10. Change of Euler angle for the base propeller during the flight.

Figure 11 presents the variation in desired and recorded altitude over time for the base propeller. This graph is crucial for assessing the stability of the UAV and how well it adhered to its intended flight path. The graph demonstrates that the UAV maintained position stability effectively while changing direction and altitude. Notably, the highest altitude deviation observed during the flight was approximately 0.24 meters, with an overall altitude deviation of just 0.1 meters.

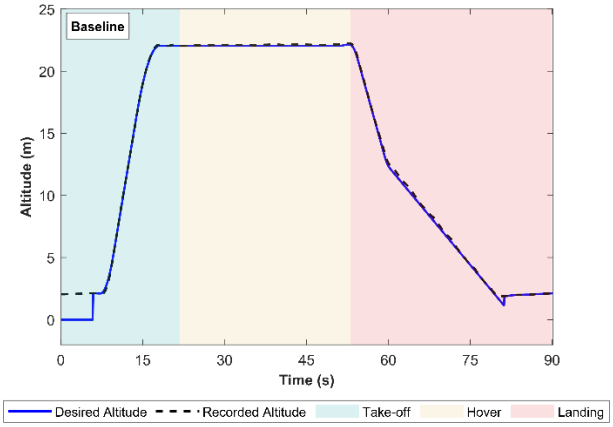

Figure 11. Change of altitude of the base propeller during the flight.

Vibration is a critical parameter used to assess the directional stability of an aircraft. The accelerometer mounted on the UAV is highly sensitive to vibrations. The UAV's position is determined by the accelerometer in conjunction with GPS and barometer sensors. Excessive vibration can disrupt the accurate determination of the UAV's position, leading to unfavorable flight conditions and potentially resulting in a crash.

Figure 12 displays the wind velocity experienced by the UAV during its flight. The wind speed was measured using the anemometer mounted on the UAV. Throughout the flight, the wind speed remained below 6 meters per second, indicating that there were no adverse effects of the wind on the UAV.

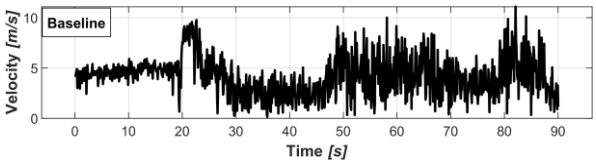

Figure 12. Wind velocity of the base propeller during the flight.

The variation in raw acceleration along the X, Y, and Z axes over time for the base propeller is depicted in Figure 13. Pixhawk specifies that the raw acceleration values should fall within the range of –3 to +3 for roll and pitch, and between +15 and –15 for yaw [31]. It is evident from the figure that the raw acceleration values for pitch, roll, and yaw remained within the desired range. Based on these results, it can be concluded that the wind did not have a detrimental impact on the UAV.

Additionally, the power consumption for the flight of the base propeller was recorded as 16.33 Wh.

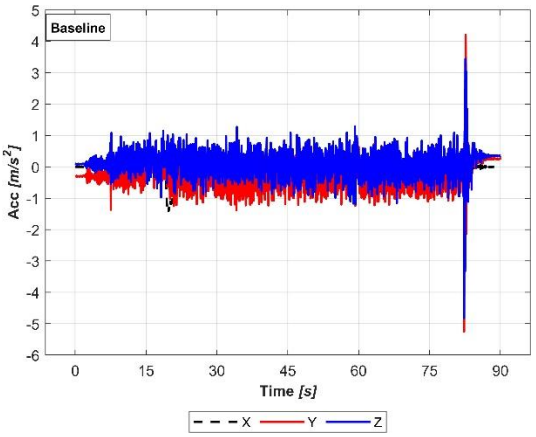

Figure 13. Change of raw acceleration of X, Y and Z for the base propeller during the flight.

4.2.2. Analysis of the test propellers

The changes in the desired and recorded Euler angles for DAE51 propellers are depicted in

Figure **14**. While a deviation occurred in the angles of roll, pitch, and yaw for the DAE51 propeller, it remained relatively low but persisted throughout the entire flight. The deviation observed for the DAE51 propeller is higher than that for the NACA4412 and NLF0115 propellers. The maximum deviation for the DAE51 propeller was recorded as 1.75° for roll angle, 2.20° for pitch angle, and 22.17° for yaw angle.

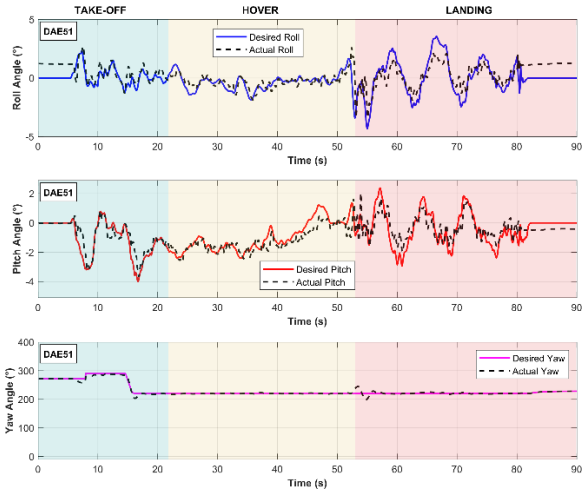

Figure 14. Change of the desired and recorded Euler angle for DAE51 during the flight.

The changes in the desired and recorded Euler angles for the MH42 propeller are illustrated in Figure 15. In the case of the MH42 propeller, the deviation between the desired and recorded Euler angles was nearly the same, with only minor differences. However, the deviations in the roll angle were particularly noticeable, especially at the beginning of take-off and during landing. At take-off, the deviation reached up to 1°, and it increased to 3° during landing. The MH42 propeller exhibited the most significant deviations in the angles of roll, pitch, and yaw. The maximum deviations were recorded as 2.4° for roll, 2.8° for pitch, and 11.18° for yaw.

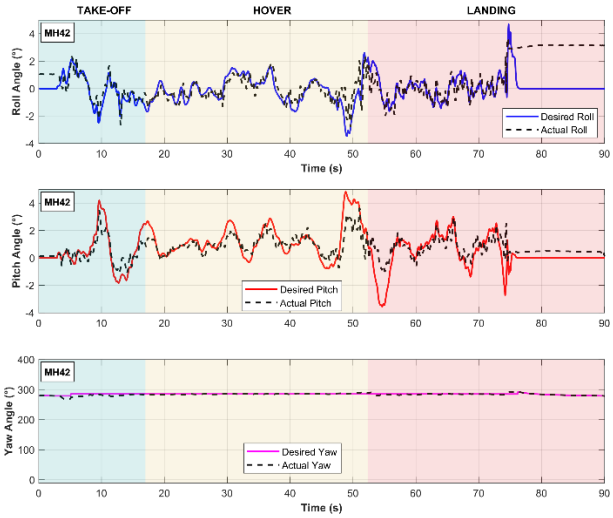

Figure 15. Change of the desired and recorded Euler angle for MH42 during the flight.

The changes in the desired and recorded Euler angles for the NACA4412 propeller are illustrated in Figure 16. It can be observed that the UAV faced difficulties in maintaining its movement at the beginning of take-off and the end of landing. However, the UAV exhibited good hovering capability and maintained its position effectively during other phases of flight. Deviations in any of the Euler angles can disrupt the stability of the UAV and affect its other orientations. Similarly, the figure reveals that there were deviations in the angles of roll, pitch, and yaw at the beginning of take-off and the end of landing. The maximum recorded deviations were 4.1° for the roll angle, 2.3° for the pitch angle, and 18.19° for the yaw angle.

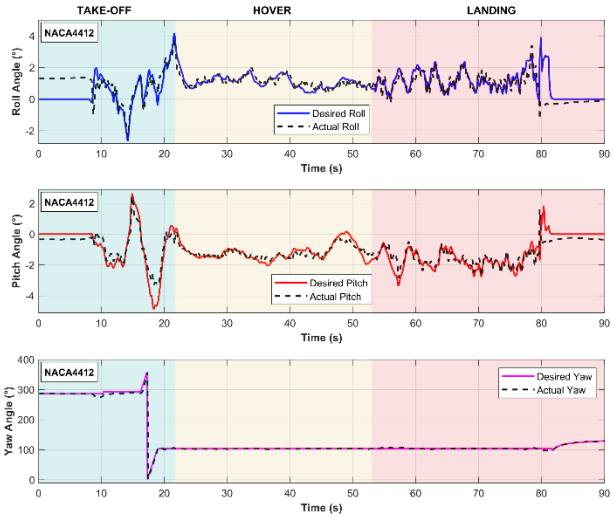

Figure 16. Change of the desired and recorded Euler angle for NACA4412 during the flight.

The changes in the desired and recorded Euler angles for the NLF0115 propeller are illustrated in Figure 17. Significant deviations in the roll angle were observed at the beginning of take-off, during some portions of hover, and at the end of landing when using the NLF0115 propeller. The figure shows that the deviation in the roll angle reached up to 5° during landing. Additionally, a similar pattern of deviation was observed for the pitch angle. The maximum recorded deviation for the NLF0115 propeller was 5.13°. Similarly, there was a disturbance in the yaw angle with a pattern similar to that of roll and pitch angles, indicating poor directional stability during landing. The maximum recorded deviations were 1.53° for pitch and 13.53° for yaw.

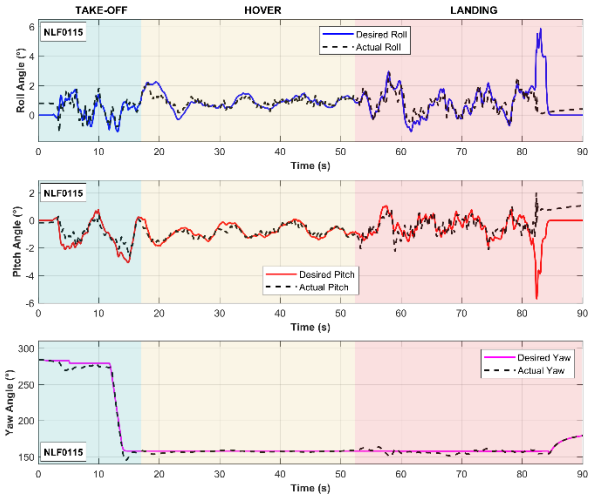

Figure 17. Change of the desired and recorded Euler angle for NLF0115 during the flight.

The altitude profiles for the designed propellers are depicted in Figure 18. Notably, DAE51 displayed minimal altitude deviation with a peak of 0.4 m and an overall deviation of 0.072 m, albeit higher than other propellers. In the case of MH42, deviations in Euler angles were observed, particularly during take-off, resulting in a peak altitude deviation of 0.57 m and an overall deviation of 0.019 m. NACA4412 demonstrated altitude data that closely aligned with expectations throughout the flight, with negligible deviations, peaking at 0.47 m and averaging around 0.031 m. Similarly, NLF0115's altitude closely matched expectations, displaying a peak deviation of 0.38 m and an overall deviation of 0.022 m, with minor differences observed.

Figure 19 presents the wind velocities experienced by the UAV during flight with the test propellers. An onboard digital anemometer allowed for real-time measurement of wind speeds impacting the UAV. This capability was crucial for distinguishing between wind-induced and propeller-induced effects on the UAV's movement. The wind speeds remained stable throughout the flight for the designed propellers. Although there were occasional instantaneous increases in wind speed, the overall impact on the UAV was minimal, with no significant adverse effects observed.

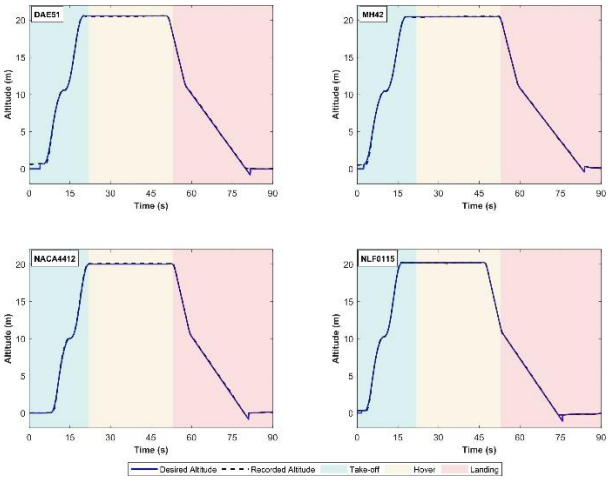

Figure 18. Change of the desired and recorded altitude for the test propellers during the flight.

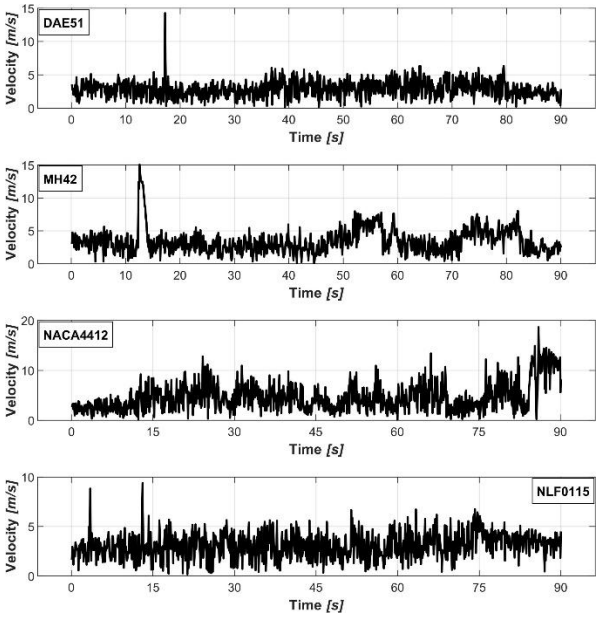

Figure 19. Wind velocity during the flight of the test propeller during the flight.

Figure 20 displays the changes in raw acceleration along the X, Y, and Z axes over time for the designed propellers. The raw acceleration values for all four propellers, DAE51, MH42, NACA4412, and NLF0115, remained within the acceptable range. This indicates that there was no significant vibration originating from either the propeller or the UAV, ensuring stable flight conditions.

Table 8 presents the power consumption data for the designed propellers during the flight tests. The power consumption for DAE51 was measured at 16.90 Wh, while MH42, NACA4412, and NLF0115 consumed 18.33 Wh, 15.18 Wh, and 15.75 Wh, respectively. Notably, MH42 exhibited the highest power

consumption, whereas NACA4412 had the lowest power consumption among the tested propellers.

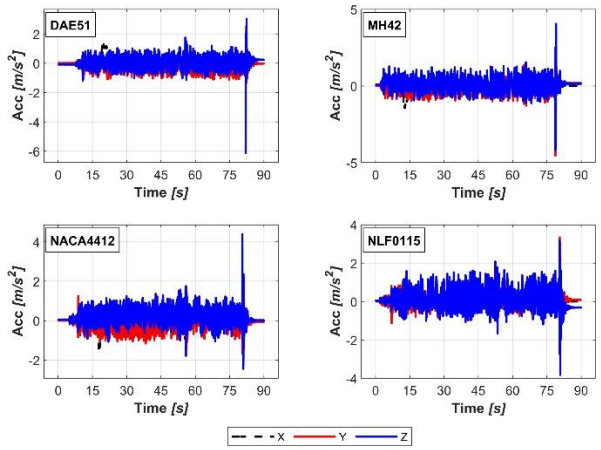

Figure 20. Change of raw acceleration of X, Y and Z for the test propellers during the flight.

Table 8. Energy consumptions of the test propellers during the flight.

Propeller	Baseline	DAE51	MH42	NACA4412	NLF0115
Energy consumption (Wh)	16.33	16.9	18.33	15.18	15.75

5. CONCLUSIONS

This study focused on designing and testing new propeller types to enhance quadcopter directional stability. Four propeller designs based on DAE51, MH42, NACA4412, and NLF0115 airfoils were developed, analyzed using CFD, and tested in real-world conditions.

The difference between the analytical and CFD calculations of thrust coefficient was found to be relatively low, with discrepancies of –3.93% for DAE51, –5.11% for MH42, –5.80% for NACA4412, and –6.73% for NLF0115. These results were considered acceptable, suggesting that the designed propellers were capable of generating the required thrust.

Experimental flight tests revealed favorable directional stability across all designs, with altitude deviations ranging from 0.019 m to 0.072 m. Energy consumption analysis provided critical insights into efficiency, with NACA4412 consuming the least power (7% less) than the base propeller. NLF0115 consumed slightly more power (3.6% less than base), while DAE51 and MH42 consumed 6.7% and 20% more power than the base propeller, respectively.

Based on comprehensive evaluation of all performance parameters, the NACA4412 propeller design demonstrated the best overall performance, offering the lowest power consumption, excellent directional stability with minimal altitude deviations (0.031 m), and acceptable Euler angle variations. The result was followed by The NLF0115 design, with slightly higher power consumption but comparable stability characteristics. While DAE51 and MH42 designs maintained acceptable directional stability. However, they consumed higher energy that makes them less suitable for applications where flight duration is a priority.

These findings highlight the potential of custom propeller designs, particularly those based on NACA4412 and NLF0115 airfoils, for optimizing quadcopter performance in terms of both stability and energy efficiency.

DECLARATION OF ETHICAL STANDARDS

The author(s) of this manuscript declare that the materials and methods used in their studies do not require ethics committee approval and/or legal-specific permission

AUTHORS' CONTRIBUTIONS

Yahya ÇELEBİ: Writing, software, validation, visualization, data collection, review and editing.

Hüseyin AYDIN: Validation, supervision, review and editing.

CONFLICT OF INTEREST

There is no conflict of interest in this study.

REFERENCES

[1] Breivik, M., Hovstein, V. E., and Fossen, T. I., "Straight-Line Target Tracking for Unmanned Surface Vehicles", ***Modeling, Identification And Control***, 29 (4): 131–149 (2008).

[2] Elmas, E. E. and Alkan, M., "Bir İnsansız Hava Aracı Sisteminin Tasarımı, Benzetimi ve Gerçekleştirilmesi", ***Politeknik Dergisi***, 26 (2): 929–940 (2023).

[3] Lim, H., Park, J., Lee, D., and Kim, H. J., "Build your own quadrotor: Open-source projects on unmanned aerial vehicles", ***IEEE Robotics & Automation Magazine***, 19 (3): 33–45 (2012).

[4] Van Tilburg, C., "First Report of Using Portable Unmanned Aircraft Systems (Drones) for Search and Rescue", ***Wilderness & Environmental Medicine***, 28 (2): 116–118 (2017).

[5] Carreno Ruiz, M., "CFD simulation of propellers: Best Practices Analysis", ***PhD Thesis***, Politecnico Di Torino, (2019).

[6] Elmas, E. E. and Alkan, M., "Collision Avoidance for Autonomous Unmanned Aerial Vehicles with Dynamic and Stationary Obstacles", ***Politeknik Dergisi***, 28 (1): 297–308 (2025).

[7] Çelebi, Y. and Aydın, H., "Multirotor Unmanned Aerial Vehicle Systems: An In-Depth Analysis of Hardware,

Software, And Communication Systems", ***Journal Of Aviation***, 9 (1): 225–240 (2025).

[8] Gunarathna, J. K. and Munasinghe, R., "Development of a Quad-rotor Fixed-wing Hybrid Unmanned Aerial Vehicle", ***2018 Moratuwa Engineering Research Conference (MERCon)***, (2018).

[9] Raimundo, A. S. L., "Autonomous obstacle collision avoidance system for uavs in rescue operations", ***Master's Thesis***, University Institute of Lisbon, (2016).

[10] Rodrigues, T. A., Patrikar, J., Choudhry, A., Feldgoise, J., Arcot, V., Gahlaut, A., Lau, S., Moon, B., Wagner, B., and Matthews, H. S., "In-flight positional and energy use data set of a DJI Matrice 100 quadcopter for small package delivery", ***Scientific Data***, 8 (1): 1–8 (2021).

[11] Su, Y., Malachuk, P., Shah, D., and Khorana, A., "Precision Differential Drone Navigation", (2022).

[12] Azizan, N. N. and Sapit, A., "Airflow Characteristic of UAV Quadcopter Propeller Blade Using Computational Fluid Dynamics (CFD)", ***Progress In Aerospace And Aviation Technology***, 2 (2): 8–16 (2022).

[13] Sanchez, R. D., "Aerodynamic and aeroacoustic design of small unmanned aircraft system propellers at low Reynolds numbers.", ***Master's Thesis***, University of Baylor, (2020).

[14] Dim, C., Nabor, F., Santos, G., Schoeler, M., and Chua, A., "Novel Experiment Design for Unmanned Aerial Vehicle Controller Performance Testing", ***2019 The 5th International Conference on Electrical Engineering, Control and Robotics (EECR 2019)***, (2019).

[15] Ghaffari, A., "Optimization of blade profiles for a coaxial drone", ***Master's Thesis***, University of Stavanger, (2021).

[16] Alabaş, H. A. and Nacakli, Y., "Unsteady 3D Computational Fluid Dynamics Simulation Of a Mini Unmanned Aerial Vehicle Propeller", ***Uluslararası Marmara Fen Ve Sosyal Bilimler Kongresi (Bahar) 2019 Bildiriler Kitabı***, (2019).

[17] Çelebi, Y., Cengiz, M., and Aydın, H., "Propeller Design of UAV Under Low Reynolds Numbers", Article and Reviews in Engineering Sciences, ***Platanus Publishing***, 407–438 (2024).

[18] Çelebi, Y. and Cengiz, M., "Verification and Validation of UAV Propeller using CFD", ***9th International Azerbaijan Congress on Life, Engineering, Mathematical, and Applied Sciences***, Azerbeycan, (2024).

[19] Özen, E., "Design of unmmanned aerial vehicle and gorund terminal", ***Master's Thesis***, University of Gaziantep, (2019).

[20] Yeong, S. P. and Dol, S. S., "Aerodynamic optimization of micro aerial vehicle", ***Journal Of Applied Fluid Mechanics***, 9 (5): 2111–2121 (2016).

[21] Williamson, G. A., McGranahan, B. D., Broughton, B. A., Deters, R. W., Brandt, J. B., and Selig, M. S., "Summary of Low-Speed Airfoil Data, Vol. 5", ***University Of Illinois, Champaign, IL***, 204: (2012).

[22] Park, D., Lee, Y., Cho, T., and Kim, C., "Design and performance evaluation of propeller for solar-powered high-altitude long-endurance unmanned aerial vehicle", ***International Journal Of Aerospace Engineering***, 2018: (2018).

[23] Carvalho, I. D. de S. B., "Low Reynolds propellers for increased quadcopters endurance", ***Master's Thesis***, University of Beira Interior, (2013).

[24] Gökdemir, M. and Ürgün, S., "Aerodynamic Analysis of Wing Profiles with Similar Roundback", ***Journal Of Aviation***, 4 (2): 25–35 (2020).

[25] Tanürün, H. E., Akın, A. G., and Acır, A., "Rüzgâr Türbinlerinde Kiriş Yapısının Performansa Etkisinin Sayısal Olarak İncelenmesi", ***Politeknik Dergisi***, 24 (3): 1219–1226 (2021).

[26] Internet: Drela, M., "Qmil and Qprop", https://web.mit.edu/drela/Public/web/qprop/qmil_doc.txt , Accessed: October 11, 2023.

[27] Internet: URL, "Ultimaker Cura: Powerful, Easy-to-Use 3D Printing Software", https://ultimaker.com/software/ultimaker-cura, Accessed: October 11, 2023.

[28] Zore, K., Caridi, D., and Lockley, I., "Fast and Accurate Prediction of Vehicle Aerodynamics using ANSYS Mosaic Mesh", ***SAE Technical Paper***, (2020).

[29] Kaya, A. F., Tanürün, H. E., and Acır, A., "Numerical Investigation of Radius Dependent Solidity Effect on H-Type Vertical Axis Wind Turbines", ***Politeknik Dergisi***, 25 (3): 1007–1019 (2022).

[30] Tanürün, H. E., Ata, İ., Canlı, M. E., and Acır, A., "Farklı Açıklık Oranlarındaki NACA-0018 Rüzgâr Türbini Kanat Modeli Performansının Sayısal ve Deneysel İncelenmesi", ***Politeknik Dergisi***, 23 (2): 371–381 (2020).

[31] Internet: URL, "Measuring Vibration — Copter Documentation", https://ardupilot.org/copter/docs/common-measuring-vibration.html, Accessed: October 11, 2023.